Simultaneous Wind and Rain Estimation for QuikSCAT at Ultra-High Resolution

Michael P. Owen and David G. Long, *Fellow, IEEE*

***Abstract*—Although originally designed solely for wind retrieval, the QuikSCAT scatterometer has proved to be a useful tool for rain estimation as well. Resolution enhancement algorithms designed for QuikSCAT allow for ultra-high-resolution (UHR) (2.5 km) simultaneous wind and rain (SWR) retrieval. The principle advantage of UHR SWR estimation is that compared to conventional resolution, the higher resolution allows for identification of much smaller rain events and their effects on the wind field. To enable SWR retrieval, we adjust the geophysical model function to account for rain effects such as attenuation and increased backscatter due to increased surface roughness. Two possible rain models are proposed, a phenomenological rain model and an effective rain model. Both models are compared by evaluating data fit and rain estimation performance. Comparisons of a co-located data set show that QuikSCAT UHR SWR integrated rain rates are comparable to those from tropical rain measuring mission precipitation radar (TRMM PR) but have higher variance. Buoy comparisons reveal improved wind estimates in the presence of rain. The theoretic estimator bounds are compared to both the simulated estimator variance and the actual estimator variance. The estimator bounds indicate that despite high-noise levels, wind and rain information is still retrievable at UHR, although certain directions have degraded estimator bounds. Both rain models are compared to truth data and are shown to have comparable performance for most rain rates. Comparison with buoy measurements shows that in the presence of rain, QuikSCAT UHR SWR wind estimates have less bias and variability than wind-only estimates. Although QuikSCAT UHR SWR rain estimates are noisier than TRMM PR rain rates, they provide a useful rain flag for QuikSCAT winds.**

***Index Terms*—QuikSCAT, resolution enhancement, scatterometry, simultaneous wind/rain retrieval, wind retrieval.**

I. Introduction

THE SeaWinds scatterometer, launched on QuikSCAT by NASA in 1999, was designed to measure wind vectors over the ocean. An orbiting scatterometer is ideally suited for remote sensing of ocean winds due to the large coverage area and regular sampling pattern made possible in low Earth orbits. Although QuikSCAT measurements are unaffected by cloud cover or time of day, accurate wind estimation requires that measurements are uncontaminated by rain.

Manuscript received May 17, 2010; revised October 21, 2010; accepted December 15, 2010. Date of publication February 6, 2011; date of current version May 20, 2011.

The authors are with Brigham Young University, Microwave Earth Remote Sensing Laboratory, Provo, UT 84602 USA (e-mail: owen@mers.byu.edu; long@ee.byu.edu).

Color versions of one or more of the figures in this paper are available online at http://ieeexplore.ieee.org.

Digital Object Identifier 10.1109/TGRS.2010.2102361

Rain is a significant problem for QuikSCAT measurements if unaccounted for, thus efforts have been made at identifying and flagging rain contamination of wind estimates [1]–[5]. Typically, rain contamination results in overestimated wind speeds and strong directional bias during wind retrieval. Rain contamination can be mitigated by simultaneously estimating the rain rate and the wind vector using a model which compensates for rain effects. Such a model and a method for simultaneous wind and rain retrieval was proposed in [6] for QuikSCAT 25-km conventional-resolution products.

Here, we discuss the application of the simultaneous wind and rain (SWR) estimation technique proposed in [6] to 2.5-km ultra-high-resolution (UHR) products produced using QuikSCAT data and a resolution enhancement algorithm [7]. UHR wind and rain estimates have a singular advantage over conventional-resolution products in that they can resolve small-scale convective rain events. Convective rain events have relatively small spatial scales and are often associated with extremely high rain rates. Conventional 25-km resolution products cannot resolve such small events and are further limited by the effects of irregular beam filling [6]. At UHR, the increased resolution allows the rain estimates to resolve rain events on a much finer scale, greatly increasing information about wind and rain dynamics. This paper adapts the SWR retrieval technique to QuikSCAT UHR by addressing temporal and spatial resolution, rain backscatter modeling, and estimation performance limits. Comparison with buoy winds show that SWR provides improved-accuracy wind estimates as well as high-resolution rain estimates.

II. QuikSCAT and TRMM Background

The QuikSCAT scatterometer measures the normalized radar cross section or backscatter from the Earth's surface using a 13.4-GHz dual-polarization rotating pencil-beam antenna. For wind retrieval, QuikSCAT observations can be categorized into four 'flavors': 1) vertically polarized (V-pol) forward-looking; 2) V-pol aft-looking; 3) horizontally polarized (H-pol) forward-looking; and 4) H-pol aft-looking. The nominal incidence angle is 46° for H-pol and 54° for V-pol. Consequently, there is an outer swath region where there are no H-pol backscatter measurements. The region where there are both V-pol and H-pol measurements is termed the inner swath and is the part of the swath where rain retrieval is possible.

Radar backscatter measurements, termed σ^o, are used to estimate wind vectors via a maximum likelihood estimation technique whereby backscatter measurements are mapped to wind vectors through a geophysical model function (GMF) [8]. When σ^o is viewed as a random variable, the GMF gives an estimate of the backscatter $\hat{\sigma^o}$, which is the expected value of σ^o given a wind speed S and relative wind direction χ, i.e.,

$$\hat{\sigma^o} = E[\sigma^o|S,\chi] = \mathcal{M}(S,\chi) \tag{1}$$

where E denotes the expectation operator, $p(\sigma^o|S,\chi)$ is the conditional probability of σ^o, and $\mathcal{M}(S,\chi)$ is the GMF.

Wind retrieval—the process of estimating the wind from the measured σ^o values—is performed for each location using a maximum likelihood estimation technique. The model for the probability of a vector of σ^o measurements $\mathbf{z}$, given a wind speed and direction is given by

$$p(\mathbf{z}|S,\chi) = \prod_k \frac{1}{\sqrt{2\pi}\varsigma_k} \exp\left\{-\frac{1}{2}\frac{(z_k - \hat{\sigma^o})^2}{\varsigma_k^2}\right\} \tag{2}$$

where the variance ς_k is a function of the wind speed and direction. Note that this model assumes that each measurement is independent. This assumption is not strictly true [9] but is a useful approximation maintained here to reduce complexity. The variance term is calculated to be

$$\varsigma^2(S,\chi) = \left(K_{pc}^2 + K_{pm}^2 + K_{pc}^2 K_{pm}^2\right)\mathcal{M}(S,\chi)^2 \tag{3}$$

where K_{pm} is the normalized standard deviation of the GMF representing the uncertainty in the model function and K_{pc} represents communication noise and can be written

$$K_{pc} = \sqrt{\alpha + \frac{\beta}{\hat{\sigma^o}} + \frac{\gamma}{\hat{\sigma^o}^2}}. \tag{4}$$

The coefficients α, β, and γ are scatterometer specific [10].

Dropping constant terms, the likelihood function of a wind vector given the measurements becomes

$$l(\mathbf{z}|S,\chi) = -\sum_k \log(\varsigma_k) + \frac{1}{2}\frac{(z_k - \hat{\sigma^o})^2}{\varsigma_k^2}. \tag{5}$$

Due to the structure of the GMF, the likelihood function typically has several local maxima each of which is a possible wind vector solution. Typically up to four of these maxima, termed ambiguities, are retained after processing [11]. Wind retrieval is the process of calculating the likelihood function and finding the local maxima. The process by which one ambiguity is selected for each wind vector cell (WVC) is termed ambiguity selection.

SWR retrieval is possible for the inner swath using QuikSCAT [6] but it requires independent data sets to properly calibrate the QuikSCAT rain model. The development of the rain model uses measured rain data provided by the tropical rain measuring mission precipitation radar (TRMM PR) as the comparison rain data set and wind products from the National Centers for Environmental Prediction (NCEP) as the comparison wind data set.

Operating at 13.8 GHz, TRMM PR provides an ideal comparison data set for rain. TRMM PR provides rain data at a 4.3–5-km resolution with a swath width of 247 km, but is limited to tropical latitudes. The model training and validation data set we use is composed of QuikSCAT and TRMM PR measurements co-located to within 10 min for the years 2000 and 2001 with over 7 000 000 2.5-km WVCs. We compare the co-located QuikSCAT 2.5-km resolution rain data to a spatially interpolated TRMM PR data set. To obtain co-located wind data, NCEP winds are interpolated spatially and temporally to match QuikSCAT resolution and measurement times. Although the NCEP wind product is inherently lower resolution than the QuikSCAT UHR product, we assume that we can compensate for any bias.

SWR retrieval for QuikSCAT was first studied and validated at conventional (25 km) resolution [6], [12]. However at UHR, several additional issues arise in SWR retrieval. Due to the signal processing implementation, QuikSCAT has essentially no range resolution with which it can differentiate between atmospheric and surface scattering. Because rain occurs up to an altitude of 6 km, the incidence angles used by QuikSCAT can cause up to 6 km of apparent horizontal spreading of the rain signal, which for UHR products is significantly larger than a resolution cell. The antenna spatial response and the resolution enhancement algorithm together result in additional horizontal spreading of the rain signal, causing rain contamination of measurements in WVCs that are near rain events. Further, at high resolution, intense rain cells have a stronger effect on the observed backscatter since there is less averaging into the resolution cells than for the 25-km product. Consequently, the conventional resolution rain model and associated assumptions may be inappropriate for the UHR case.

III. UHR Rain Model

The addition of a rain model to the GMF is the principle difference between conventional wind retrieval and SWR estimation. Thus, the accuracy of the SWR estimates depend upon the suitability of the rain model. Falling hydrometeors introduce several changes in the observed radar backscatter which must be accounted for in the model. Rain striking the ocean surface increases the surface roughness and observed backscatter [13]. Atmospheric hydrometeors also cause attenuation of the surface backscatter signal in addition to volume scattering from the raindrops themselves. This attenuation can occur in two forms, atmospheric attenuation of the surface backscatter and attenuation of the wind-induced surface waves by intense rain [14]. Since the wave attenuation only occurs during the most intense rain events, we do not include a separate term in the rain models for this effect. To account for these effects, we adopt a simple model

$$\sigma_o = (\sigma_w + \sigma_{sr})\alpha_r + \sigma_r \tag{6}$$

where σ_o is observed backscatter, σ_w is the wind-only (WO) backscatter, σ_{sr} is the surface backscatter due to rain, α_r is the attenuation caused by rain, and σ_r is the backscatter from falling rain drops. This model is referred to in the following as the phenomenological rain model.

A modification of the above phenomenological model was adopted in [6] and [15]. This modified rain model assumes that the additive backscatter terms due to rain can be combined to form an effective rain backscatter model

$$\sigma_o = \sigma_w \alpha_r + \sigma_e \tag{7}$$

where σ_e is the effective rain backscatter which approximates $(\sigma_{sr}\alpha_r + \sigma_r)$ from the phenomenological model.

At UHR, the effects of localized intense rain cells are magnified when compared to the effects at 25- km resolution. Thus, the rain model must accurately portray the backscatter effects of intense rain events. Here, we evaluate both the phenomenological and effective rain models as applied to UHR wind and rain retrieval. There are differences in wind and rain retrieval due to rain model choice which may be attributed to the combined effects of the surface backscatter and atmospheric attenuation. If, for instance, the atmospheric attenuation dominates the surface backscatter, then the effective rain model may be a sufficient characterization of the rain effects. However, the effects of atmospheric attenuation and backscatter vary widely as a function of rain rate; thus, the phenomenological model may be more appropriate for UHR.

The rain model parameters are estimated for QuikSCAT using the two independent data sets discussed previously, NCEP winds and TRMM PR rain rates. There are several effects due to both the spatial and temporal differences of the QuikSCAT and TRMM PR observations which are detrimental to the rain model if not considered. We discuss these effects in the following two subsections before discussing the rain models themselves.

A. Spatial Resolution

Although QuikSCAT UHR products are reported at 2.5 km, the effective resolution is somewhat lower due to the limitations of the σ^o resolution enhancement process [9]. When using TRMM PR rain rates to estimate the effective rain backscatter, the resolution enhancement can have significant consequences. The resolution-enhanced backscatter used to produce UHR products is reconstructed from irregular spatial samples [7]. The reconstruction process creates a backscatter field by averaging the observations that overlap a single resolution cell. The antenna spatial response function is larger than a resolution cell so the backscatter in a single resolution cell is an irregular contribution of the backscatter from the surrounding area. Such averaging is often appropriate for wind events, which have smoother spatial scales. For rain events, which can have rapid spatial variation, it is important to account for the effects of the reconstruction process.

To ensure compatible rain observations for TRMM PR and QuikSCAT, we interpolate the measured TRMM PR rain field to the resolution of QuikSCAT UHR products. The interpolated rain field is then "sampled" with a simplified antenna pattern in two steps using the QuikSCAT measurement geometry and spatial response function [16] for each observation flavor. First, an estimate of the rain rate observed by each QuikSCAT slice measurement is obtained for each of the G_i slice measurements using

$$R(G_i) = \frac{\sum_{(a,c)\in G_i} R_{TRMM}(a,c)}{\sum_{(a,c)\in G_i}} \tag{8}$$

where $R(G_i)$ is the average TRMM-observed rain rate in the along- and cross-track cells (a, c) that contribute to the slice measurement G_i. After estimating the rain rate observed by each QuikSCAT measurement, the measurements that overlap each along- and cross-track cell (a, c) are averaged to mimic the resolution enhancement process using

$$R_{PL}(a,c) = \frac{\sum_{G_i\in H_{PL}(a,c)} R(G_i)}{\sum_{G_i\in H_{PL}(a,c)}} \tag{9}$$

where $H_{PL}(a, c)$ is the set of measurements G_i of a given polarization P and look direction L which overlap the along- and cross-track location (a, c). $R_{TRMM}(a, c)$ is the TRMM PR-measured rain rate after spatial interpolation to the QuikSCAT resolution. $R_{PL}(a, c)$ is the TRMM PR rain rate after QuikSCAT resolution enhancement corresponding, respectively, to each polarization and look direction. There are four rain fields: R_{VA}, R_{VF}, R_{HA}, and R_{HF}, corresponding to the V-pol aft look, V-pol forward look, H-pol aft look, and H-pol forward look, respectively.

The four resulting rain fields are directly comparable to the resolution-enhanced backscatter fields used to produce UHR wind products. This process is essentially identical to the resolution enhancement algorithm used to produce UHR products [7]. These "resolution-enhanced" TRMM PR rain fields thus represent the rain rate observed by QuikSCAT at UHR. The major difference between the TRMM PR-observed rain field and the rain rates observed by QuikSCAT is that due to the large sampling aperture and the resolution enhancement process of QuikSCAT, the QuikSCAT-observed rain fields are a low-pass filtered version of the TRMM PR observations.

When rain events do not uniformly fill the antenna beam, the rain rate corresponding to the measured backscatter may be misrepresented. This effect is commonly referred to as irregular beam filling. The interpolation and resampling of rain rates described above simplifies the beam-filling problem since the rain rate in each WVC after the above sampling process is the QuikSCAT observed rain rate. Using the QuikSCAT-observed rain in each cell accounts for the effects of irregular beam filling, thereby reducing variability in the rain backscatter models.

One additional source of variability between the TRMM PR and QuikSCAT observations is the very different incidence angles. TRMM PR is designed to observe nearly vertical rain columns, whereas QuikSCAT operates at an incidence angle of 46° or 54°. Since rain frequently occurs above 5 km and QuikSCAT has limited-range resolution, the rain signal may appear in multiple resolution cells. This effect is relatively small compared to the resolution enhancement process and thus we do not explicitly compensate for it in the remainder of this paper.

B. Temporal Resolution

Temporal effects are particularly important for QuikSCAT UHR rain products due to the rapid temporal variations involved in rain dynamics. There are two general classes of rain events, stratiform and convective, each of which has a different character. Most stratiform rain events have large spatial scales and low to moderate rain rates throughout. These large rain events are typically associated with slow-moving storm systems. Convective rain events such as microbursts and macrobursts however, typically have small spatial scales and short durations, on the order of 10 min [17], and are typically associated with intense fast-moving storms [18]. Additionally, the highest observed rain rates are associated with these types of storms.

Because of the dynamic nature of rain events, there are two fundamental temporal effects which must be addressed to meaningfully compare QuikSCAT and TRMM PR observations at UHR. First, the observation times of QuikSCAT and TRMM PR differ due to very different orbit geometries. For stratiform rain events, a small difference in observation time has a relatively low impact on the rain backscatter estimates since the events are large and move slowly. However, convective rain events can have such rapid dynamics that the rain event can significantly change and move multiple resolution cells between the TRMM PR and QuikSCAT observation times. Since convective rain events are typically associated with high rains, if the observation time differences due to orbit geometry are unaccounted for, the effects of high rain on QuikSCAT observations may be misrepresented.

In addition to observation time differences due to different orbit geometries, there are observation time differences that can be uniquely attributed to the QuikSCAT sampling geometry. Although a single observation time is reported with the conventional-resolution wind estimates for each QuikSCAT location, these times are, in reality, averages. Due to the helical sampling pattern and different incidence angles, QuikSCAT has observation times for a fixed location which range over a window as large as 4.5 min. For example, near the nadir track, the V-pol forward- and aft-looking measurements of the same location are made 4.5 min apart. Thus, in many cases, intense rain events can move through several 2.5- km resolution cells within the QuikSCAT observation window. This means in essence that each observation type (forward V and H, aft V, and H) views a slightly different rain field. Typically, the differences in the rain fields are small and consist of a spatial shift due to the motion of the rain event. This effect is small for low to moderate rain events which typically have large spatial scales and smaller variability, but for high–intense rain events, it can cause discrepancies in the rain backscatter estimates.

In this paper, we use a simple approximation to reduce the effects of temporal differences between the QuikSCAT and TRMM PR observations. Because scatterometer σ^o observations of a given flavor have similar measurement times which differ from other flavors, we assume that there is constant spatial shift in the TRMM PR observed rain events for each QuikSCAT observation flavor. This constant shift can be interpreted as the entire rain field moving a fixed amount between the TRMM PR observation time and the observation time for the QuikSCAT flavor of interest. Although this does not fully account for realistic rain dynamics, it is a first-order correction.

A simple way to estimate the fixed shift for each QuikSCAT measurement flavor is to use the 2-D cross correlation between the array R_{PL} from (9) and the rain backscatter estimates as calculated in the following sections. The location of the maximum value of the cross correlation gives the shift required to maximally correlate the TRMM PR rain fields to the rain backscatter estimates. Typically, the required data shift is between 2.5 and 7.5 km or one to three resolution cells. As might be expected, the shifts for the forward-looking observations are similar for both polarizations as the observation time difference is small for identical look directions. Although the shifts are just a few UHR WVCs, correcting for the shift in the data substantially reduces the variability of the rain backscatter estimates as a function of the observed rain rate, particularly for high rain rates.

C. Attenuation Model

The atmospheric attenuation factor α_r model can be estimated directly using TRMM PR measurements of path-integrated attenuation. Note that the path-integrated attenuation pia measured by TRMM PR reflects the path specified by the TRMM PR geometry and must be adjusted for QuikSCAT geometry which has a longer path due to the change in incidence angle. The QuikSCAT pia estimates are modeled using

$$pia(R_{dB}, p) = 10^{\sum_{k=0}^{2} R_{PL_{dB}}^{k} p_k/10} \tag{10}$$

where $R_{PL_{dB}}$ is the resolution-enhanced TRMM PR rain rate in dB, and a_k are the model coefficients. Path-integrated attenuation is related to α_r according to

$$\alpha_r(R_{dB}, p) = 10^{-pia(R_{dB},p))/10}. \tag{11}$$

Fig. 1 shows the attenuation factor α_r, rain rate from TRMM PR, and the resulting quadratic attenuation model for each polarization. In reality, the atmospheric attenuation may be polarization dependent; however, since TRMM PR reports only a single polarization, we assume for lack of a better model, that the path-integrated attenuation is identical for each polarization and only varies due to the difference in path lengths for each polarization.

The model coefficients p_k of the atmospheric attenuation factor are estimated by first performing a kernel-smoothing operation on the data. The resulting nonparametric fit is shown with the data in Fig. 1. The model coefficients are estimated using a linear least-squares approach of the nonparametric fit in log space. The values of a_k estimated in this manner are listed in Table I. This approach avoids the limitations of a direct nonlinear least-squares approach. Due to the relative simplicity and robustness of this method, this fitting technique is used throughout the remainder of this paper to determine each set of model coefficients.

The atmospheric rain attenuation is identical in both the effective and phenomenological rain models. The other model

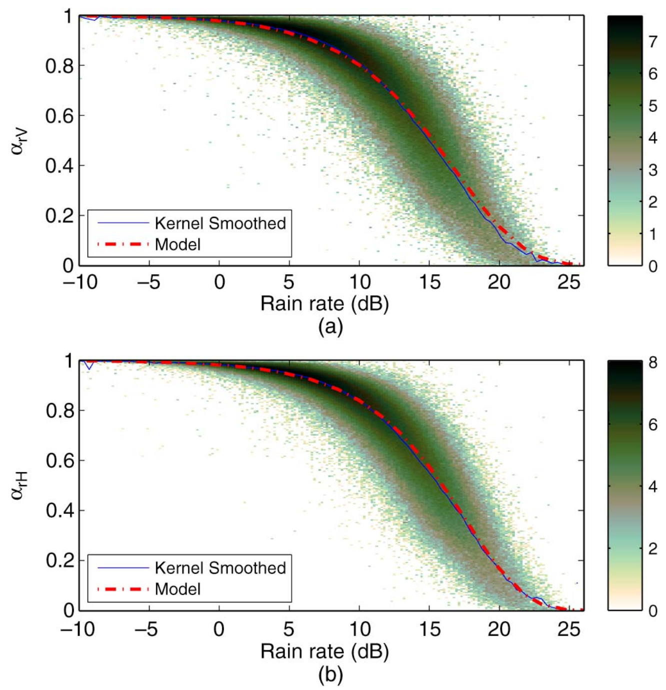

Fig. 1. Rain attenuation models for (a) V and (b) H polarizations. The background color is the path attenuation data measured by TRMM PR adjusted for the QuikSCAT propagation geometry which is used to derive the models. Note that the background color is the log of the scatter density which is shown in the plot to accentuate less common rain rates. This, however, increases the apparent variance.

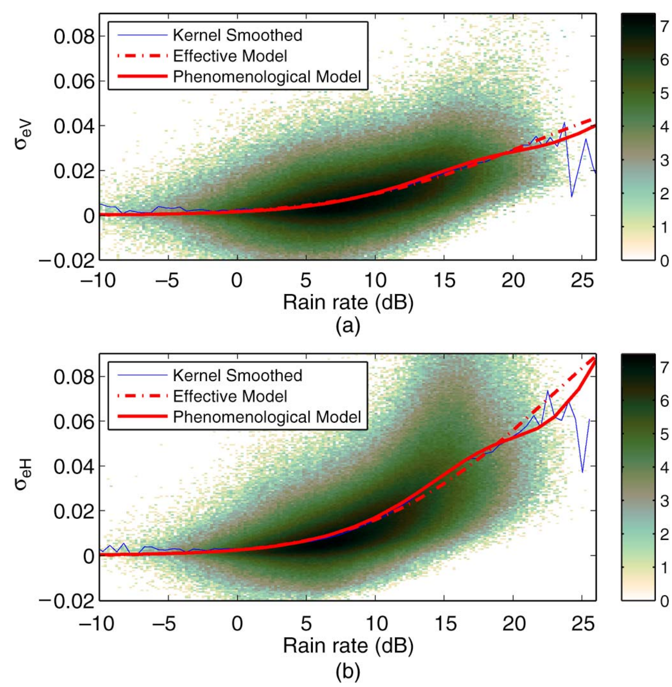

Fig. 2. Effective rain backscatter σ_e models for (a) V and (b) H polarizations. The background color is the log of the scatter density of estimated σ_e used to derive the model for both polarizations. Note that there is significant variance in the data used to derive the model.

TABLE I
RAIN MODEL PARAMETERS

Polarization	Parameter	k=0	k=1	k=2
H	p_k	-10.92	0.95	0.001824
V	p_k	-10.02	1.01	-0.0030
H	e_k	-26.08	0.94	-0.013
V	e_k	-27.36	0.84	-0.012
H	a_k	-35.83	1.39	-0.016
V	a_k	-37.9	1.48	-0.022
H	s_k	-26.67	0.84	
V	s_k	-28.42	0.78	

terms and parameters are different and are derived and estimated below. The following subsections discuss the estimation of the parameters for each model and then discuss the differences between the models.

D. Effective Rain Model

To estimate the effective backscatter model, we use (7) and solve for σ_e. Thus

$$\sigma_e(R_{dB}, p) = \sigma_o - \sigma_w \alpha_r \tag{12}$$

where α_r is the TRMM PR-measured atmospheric attenuation, $\sigma_w = \mathcal{M}(\mathbf{w}_{NCEP})$ is the estimated backscatter induced by the NCEP wind vector $\mathbf{w}_{NCEP}$, and σ_o is the QuikSCAT-measured backscatter value for the corresponding observation flavor. Due to noise inherent in each of the data sets, some σ_e estimates are negative. This is particularly true for low rain rates where the rain backscatter may be small. Although these negative values are not realistic, if they are discarded, they can cause severe bias in the rain model.

The scatter densities of the effective rain backscatter estimates are shown for both H and V polarizations in Fig. 2 as a function of the TRMM PR-measured rain rates. Note that the H-pol measurements are more sensitive to rain than V-pol for moderate to high rain rates.

To model the effective backscatter, we use a quadratic model of the form [6]

$$\sigma_e(R_{dB}, p) = 10^{\sum_{k=0}^{2} R_{dB}^k e_k / 10} \tag{13}$$

where e_k are the model parameters. The model parameters e_k are determined using the kernel-smoothing and linear least-squares technique outlined previously. The nonparametric kernel-smoothed fit is shown with the resulting quadratic model for each polarization in Fig. 2. The resulting model parameters are found in Table I.

It is important to note that there is an apparent noise floor in the effective rain backscatter estimates. For low rain rates (below 5 dB km-mm/hr), the variability between the NCEP model winds and QuikSCAT observations entirely dominates the rain signal, creating an apparent noise floor at about 0.001 in the σ_e estimates. This noise floor is not a physical effect as the rain backscatter decreases as the rain decreases. Thus, to estimate the effective rain model parameters, we ignore effective rain backscatter estimates for rain rates below 5 dB km-mm/hr.

E. Phenomenological Model

To estimate the backscatter models for σ_{sr} and σ_r, requires additional information from TRMM PR. TRMM PR-measured reflectivity is available in TRMM 1C21 files. The TRMM PR total atmospheric backscatter $\sigma_{r(PR)}$ can be calculated from the measured reflectivity Z_m using

$$\sigma_{r(PR)} = \int_0^{r_{nc}} 10^{-10} \frac{\pi^5}{\lambda_0^4} |K_w|^2 Z_m(r) dr \tag{14}$$

where r_{nc} is the no-clutter range, λ_0 is the wavelength in cm, $|K_w|^2$ is a coefficient relating the absorption properties of water (assumed to be 0.9), and $Z_m(r)$ is the TRMM PR-measured reflectivity for the range r [19].

The TRMM PR atmospheric backscatter $\sigma_{r(PR)}$ is adjusted for the QuikSCAT resolution and sampling by spatially interpolating to the QuikSCAT resolution followed by spatial averaging using (8) and (9). The TRMM PR observations are adjusted for the QuikSCAT geometry by compensating for the change in path lengths due to the change in incidence angle from TRMM PR to QuikSCAT.

Although TRMM PR makes H-pol atmospheric backscatter measurements, they are not directly comparable to QuikSCAT H- or V-pol atmospheric backscatter estimates. This is primarily due to the large difference in incidence angle which significantly affects the backscatter. This is a serious limitation to creating an appropriate model since there can be a significant difference in the backscatter response as a function of incidence angle and polarization. This change can be largely attributed due to the non-spherical nature of falling rain drops.

We compensate for this polarization and incidence angle sensitivity using a simple correction factor γ_p for each polarization p. The polarization-corrected QuikSCAT-observed atmospheric backscatter σ_{rp}, where p indicates polarization, can be modeled

$$\sigma_{rp} = \gamma_p \sigma_{r(PR)} \tag{15}$$

where γ_p is the polarization and incidence angle correction factor and $\sigma_{r(PR)}$ is the TRMM PR-observed atmospheric backscatter after adjusting for QuikSCAT sampling and path length changes. Utilizing this simple correction factor assumes that the difference between H and V polarization atmospheric scatter is not dependent on rain rate. In reality, the correction factor γ_p may be dependent on rain rate. However, since information to create a more informed model is unavailable, we opt to use the correction factor assumption despite its limitations. We discuss estimation of the correction factor later.

After polarization correction, the QuikSCAT-observed σ_r can be modeled for each polarization using

$$\sigma_r(R_{dB}, p) = 10^{\sum_{k=0}^{2} R_{PL_{dB}} a_k / 10} \tag{16}$$

where a_k are the model coefficients. The model coefficients are determined by fitting the model to the kernel-smoothed data. The resulting model as a function of integrated rain rate in dB is plotted together with the data used to derive the model in Fig. 3.

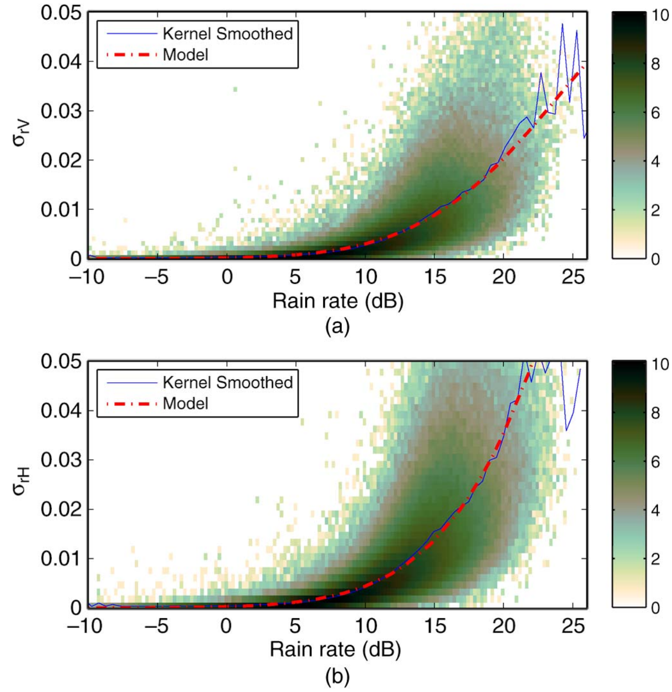

Fig. 3. Atmospheric backscatter, σ_r, with polarization correction as a function of measured rain rate for (a) V and (b) H polarizations. Note that although there is insufficient data to determine the rain model for the highest rain rates, it is anticipated that the atmospheric backscatter continues to increase with rain rate. The background color shows the log of the scatter density of the estimates.

Using the QuikSCAT-sampled atmospheric backscatter, we can form estimates of the rain-induced surface backscatter by solving (6) for σ_{sr}

$$\hat{\sigma}_{sr} = (\sigma_m - \sigma_{rp})\alpha_r^{-1} - \hat{\sigma}_w \tag{17}$$

where σ_m is the QuikSCAT-measured backscatter, σ_{rp} is the measured atmospheric rain backscatter after polarization correction, α_r is the measured rain attenuation, and $\hat{\sigma}_w$ is the estimated wind backscatter corresponding to the NCEP wind vector. Here, we have assumed that the surface backscatter due to rain is not dependent on the wind speed as demonstrated in [13].

The rain-induced surface backscatter model is written

$$\sigma_{sr}(R_{dB}, p) = 10^{\sum_{k=0}^{1} R_{PL_{dB}} s_k / 10} \tag{18}$$

where s_k are the model coefficients which best fit the kernel-smoothed data. Fig. 4 shows the estimated σ_{sr} data in addition to the kernel-smoothed fit and the resulting model. Unlike the other parts of the rain model, only two parameters are used in the surface backscatter model. A two-parameter model is more appropriate since the surface backscatter is prone to noise for both low rains due to the noise floor and high rains due to atmospheric attenuation. Thus, it is not clear that a quadratic model is justified, so we adopt a simpler linear model instead.

It is interesting to note that the rain-induced surface backscatter can be negative. This is largely due to the fact that the rain drops striking the ocean surface can cause destructive interference with the wind-induced wave field, thereby reducing

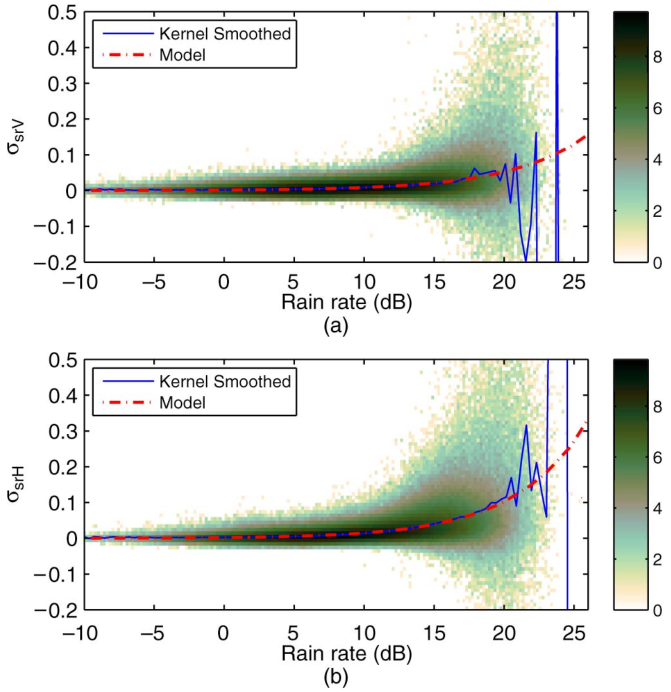

Fig. 4. σ_{sr} as a function of rain rate in decibels for (a) V and (b) H polarizations. Note that H-pol is more sensitive to the surface backscatter due to rain. The background color is the log of the scatter density of the data.

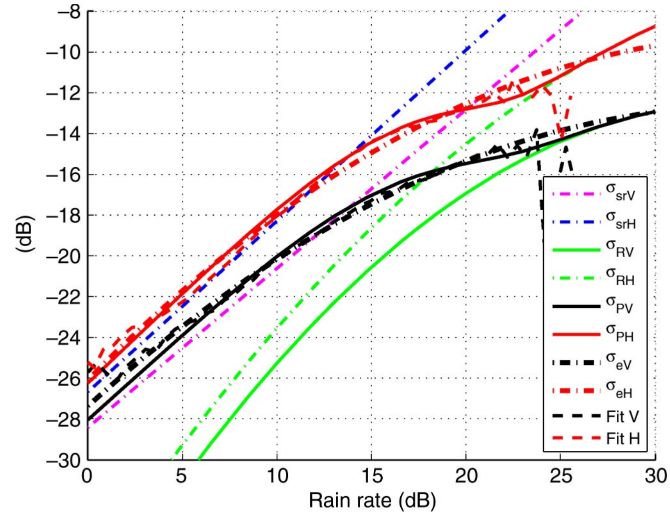

Fig. 5. Effective and phenomenological rain models for both H and V polarizations. Also included is the kernel-smoothed fit of the effective rain model data. Note that the plots include intense rain rates above 20 dB km-mm/hr where there are few observations in the data. This can give some insight on whether the model approach is reasonable.

the overall backscatter. As indicated by the models, the rain-induced surface backscatter generally increases as a function rain rate. However, for moderate to high rain rates, the variability in the data suggests that the uncertainty is high. This is consistent with the increase in atmospheric attenuation. As attenuation increases, the ability to observe and estimate the surface backscatter decreases as the overall rain backscatter becomes dominated by atmospheric scattering.

The noise level in the estimates of the rain-induced surface backscatter is readily apparent for high rain rates where attenuation is dominant. While not apparent in Fig. 4, there is a similar effect for low rain rates. As with the effective rain backscatter estimates for low rain rates, the NCEP wind variability dominates the rain signal, causing an effective noise floor in the estimates of the rain-induced surface backscatter. Such a noise floor is not a physical phenomenon as the rain-induced surface backscatter should decrease to zero as rain rate decreases. To appropriately reflect this low rain effect in the surface backscatter model, we ignore the σ_r estimates below 5 db km-mm/hr just as we did for the effective backscatter model. Thus, the surface backscatter models decrease indefinitely as rain rate decreases.

Up to this point, we have not discussed how the polarization correction coefficient γ_p can be estimated. Without additional information, one simple way to estimate the correction factor is to perform a nonlinear least-squares optimization for γ_p to minimize the error between the combined phenomenological model $\alpha_r\sigma_{sr} + \sigma_r$ and the kernel-smoothed σ_e data. Such an approach is appropriate since the phenomenological model should have similar features to the σ_e. Estimating γ_h and γ_v in this manner leads to estimates of 0.92 and 0.49, respectively. These values indicate that the QuikSCAT-observed atmospheric backscatter is slightly smaller than that observed by TRMM PR for H-pol and almost half than that observed by TRMM PR for V-pol. The corrected rain model is shown for each polarization together with the σ_e data in Fig. 2.

F. Model Comparisons

Before a more careful evaluation of the rain model uncertainty, we consider the differences between the effective and phenomenological rain models. QuikSCAT is not capable of directly discerning between the surface and atmospheric effects of rain; thus, the lumped effects of rain backscatter are most important. To understand the combined effects of both surface and atmospheric rain backscatter on the QuikSCAT-observed rain backscatter, we can compare the rain models with the kernel-smoothed fit of the effective backscatter estimates. Such a comparison is made in Fig. 5, which shows the backscatter for the kernel-smoothed fit of the effective backscatter data, the effective rain model, and the phenomenological rain model.

As indicated in Fig. 5, both the effective and phenomenological rain models match the kernel-smoothed data for low to moderate rain rates. For high to extreme rain rates (above 20 dB km-mm/hr), the effective rain model slightly overestimates the kernel-smoothed data, although the phenomenological rain model still fits well. This is a consequence of several factors but can largely be attributed to the effects of rain attenuation.

To help illustrate the effects of rain attenuation, Fig. 5 shows the surface- and atmospheric-scattering components of the phenomenological rain model. For low to moderate rain rates, the surface-scattering terms match the kernel-smoothed data well, indicating that the rain backscatter is dominated by surface scattering. For these rain rates, the atmospheric backscatter has a negligible effect since it is 10 dB lower. While the surface backscatter continues to increase with rain rate, the effective backscatter does not since the atmospheric attenuation begins to dominate the surface scatter as the rain rate exceeds

15 dB km-mm/hr. As the transition occurs from surface to atmospheric dominance, the effective rain backscatter model no longer matches the effective backscatter data. For this region, the effective rain backscatter model overestimates the rain backscatter since it does not properly describe the increased effects of rain attenuation.

Despite the fact that the rain attenuation is not explicitly accounted for in the effective rain model, the effective rain backscatter models the effects of rain on the backscatter quite well for low to moderate rain rates. Unfortunately for moderate to high rain rates, the model misrepresents the backscatter effects. Thus, from a modeling perspective, if moderate to high rain rates are of interest, then the phenomenological rain model is a more appropriate choice despite some additional model complexity.

IV. Simultaneous Wind and Rain Retrieval

SWR retrieval is accomplished using maximum likelihood estimation to estimate the wind vector and rain rate that produce the observed backscatter. SWR retrieval differs from WO retrieval in that the combined rain effect model is used instead of the WO model. The combined rain effect model is obtained by substituting the wind GMF $\mathcal{M}(S,\chi)$ for σ_w in (7) where S is the wind speed and χ is the relative wind direction. The combined wind and rain model can then be written

$$\mathcal{M}_R(S,\chi,R) = \mathcal{M}(S,\chi)\alpha_r(R) + \sigma_e(R) \tag{19}$$

where $\alpha_r(R)$ and $\sigma_e(R)$ are the quadratic rain model terms and R is the rain rate in dB km-mm/hr. Note that $\sigma_e(R)$ can be the effective rain model or the lumped term phenomenological rain model. The log-likelihood equation can be written as

$$l(\mathbf{z}|S,\chi,R) = -\sum_k \ln(\varsigma_k) + \frac{1}{2}\frac{(z_k - \mathcal{M}_r(S,\chi,R))^2}{\varsigma_k^2} \tag{20}$$

where $\mathbf{z}$ is the vector of measured σ_o values, k is the measurement index, and ς_k is the model variance. The conventional WO variance model can be modified to account for the additional variability due to rain by using the approximation from [6]

$$\varsigma_k^2 \approx (\mathcal{M}_k\alpha_{rk}K_{pm} + \sigma_{ek}K_{pe})^2(1+\alpha) + \alpha\mathcal{M}_{rk}^2 + \beta\mathcal{M}_{rk} + \gamma \tag{21}$$

where K_{pe} is the normalized standard deviation of the rain model. This approximation to the variance is independent of the rain model choice as K_{pe} can be estimated for both the effective rain model and the phenomenological rain model. For the phenomenological rain model, the effective K_{pe} is estimated by lumping the effective variance of the $\sigma_{sp}\alpha_r + \sigma_{rp}$ into the K_{pe} term.

A. Estimating K_{pe} for Retrieval

Due to variability in the NCEP wind data and temporal variability between QuikSCAT and TRMM PR observations, estimating K_{pe} from the rain backscatter is problematic and tends to overestimate the true value of K_{pe} for both rain models. As an example, consider the lowest rain rates. For these rain rates, the rain signal is quite small and the NCEP variability masks any variability due to rain. Similarly, for low to moderate rain rates, this additional noise dominates the rain model uncertainty. As the rain signal increases in strength, the variability from the NCEP winds becomes less pronounced and the apparent rain backscatter variability drops.

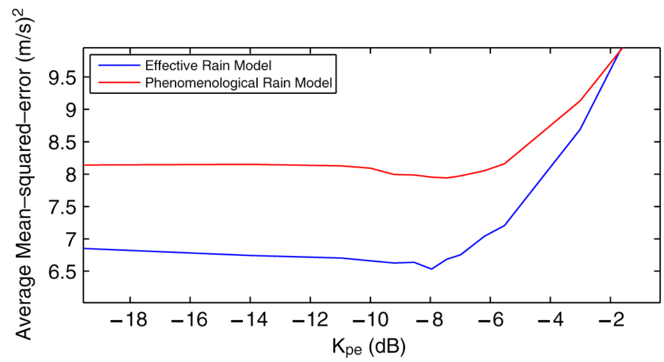

Fig. 6. Average squared error between SWR wind estimates and NCEP model winds as a function of the retrieval K_{pe} value. Note that the best value for K_{pe} is different for the effective and phenomenological rain models.

Attributing all of the additional variability to the rain model is particularly problematic when attempting to perform SWR retrieval. In many cases, the variability attributed to the rain effects is so large that it is not possible to reasonably estimate rain rate. This consequently increases the variability of the rain-contaminated wind estimates. One way to overcome this limitation is to use a fixed value for the rain model K_{pe} as in [6].

A simple way to estimate K_{pe} is to perform SWR retrieval on simulated backscatter data using candidate values for K_{pe}. The ideal K_{pe} value is that which minimizes the squared error between the wind estimates and the NCEP model winds. Unfortunately, the effects of the NCEP model wind variability are unavoidable when calculating the squared error of the wind estimates. To reduce the effects of NCEP variability, we evaluate the candidate K_{pe} values on 75 different QuikSCAT and TRMM co-located observation sets. The average squared error between NCEP and SWR wind estimates is calculated for all observations where TRMM PR observed a non-zero rain rate. The average for all of the colocations is shown as a function of K_{pe} in Fig. 6.

As indicated in Fig. 6, the values of K_{pe} of 0.16 and 0.18 for the effective and phenomenological rain models, respectively, minimize the wind squared error. While the minimum in Fig. 6 is more pronounced for the effective rain model, the wind variability using the phenomenological rain model is not particularly sensitive to the value of K_{pe}. Thus, it is reasonable to let K_{pe} be 0.16 for both the effective and phenomenological rain models. It is interesting to note that this is the same K_{pe} value as in conventional-resolution wind and rain retrieval [6]. Thus, the rain model variability is not dependent on the retrieval resolution.

V. Model Comparison

This section evaluates the accuracy of SWR estimation using both rain models using a theoretical bound and then evaluates the performance on real data against TRMM PR rain rates.

A. Cramer–Rao Bound

The Cramer–Rao lower bound (CRLB) provides a lower bound on the variance of an unbiased estimator. Wind and rain estimates are slightly biased due to nonlinearities in the model function as well as the noise level of the observations. The CRLB for biased wind and rain estimates can be written

$$E\left[(\hat{\mathbf{w}}-\mathbf{w})(\hat{\mathbf{w}}-\mathbf{w})^T\right] \geq \frac{\partial E[\hat{\mathbf{w}}]}{\partial \mathbf{w}} J^{-1}(\mathbf{w}) \left[\frac{\partial E[\hat{\mathbf{w}}]}{\partial \mathbf{w}}\right]^T \quad (22)$$

where $\hat{\mathbf{w}}$ is the wind and rain estimate and $\mathbf{w}$ is the true wind and rain vector. $J(\mathbf{w})$ is the Fisher information matrix with components J_{ij} which can be expressed as

$$J_{ij} = \sum_{k=1}^{4} \frac{\partial \mathcal{M}_{rk}}{\partial w_i} \frac{1}{\varsigma_k^2} \frac{\partial \mathcal{M}_{rk}}{\partial w_j} + \frac{\partial \varsigma_k^2}{\partial w_i} \frac{1}{2\varsigma_k^4} \frac{\partial \varsigma_k^2}{\partial w_j} \quad (23)$$

where k indexes each observation, $\mathcal{M}_{rk}$ is the wind and rain model for the wind and rain vector $\mathbf{w}$, and ς_k^2 is the observation variance [20].

It is relatively straightforward to calculate the Fisher Information matrix for a given wind and rain vector. However, since there is no analytical form for the wind and rain estimate $\hat{\mathbf{w}}$, there is no analytical form for the partial derivatives used to calculate the CRLB for a biased estimator. One method to approximate the partial derivative $\partial E[\hat{\mathbf{w}}]/\partial \mathbf{w}$ was proposed in [20]; however, the noise level in high-resolution data makes it numerically unstable for some wind vectors. Instead, we adopt an alternative approach by estimating $E[\hat{\mathbf{w}}]$ directly using Monte Carlo simulations. This approach is a more reliable alternative, provided the simulations are representative of the true wind and rain estimation performance.

B. Wind and Rain Backscatter Simulation

Backscatter due to wind can be simulated using the scatterometer noise model and the GMF. Rain backscatter is slightly more complicated since both candidate rain models are approximations to the observed rain backscatter. There are two methods which could be adopted to simulate rain backscatter. First, we could simply use the rain backscatter model as both the forward and backward rain model. For example, the simulated backscatter values could be given directly by the effective rain model, then after noisy simulation, the effective backscatter model could be used in the wind and rain retrieval process.

The second method to simulate rain backscatter, which we adopt here, is to generate the rain backscatter directly from the nonparametric kernel-smoothed fit of the rain backscatter observations (see Fig. 5). Wind and rain retrieval is then performed on the simulated backscatter data using either the effective or phenomenological rain models. An advantage of this approach is that it allows the simulated backscatter to closely resemble observed backscatter data. Since both rain models are an approximation to the observed backscatter, modeling the rain backscatter from the observed performance allows the retrieval results to realistically account for deviations between the observed rain backscatter and the model. Thus, the overall retrieval performance using each model closely mimics the estimation performance when used on actual backscatter data.

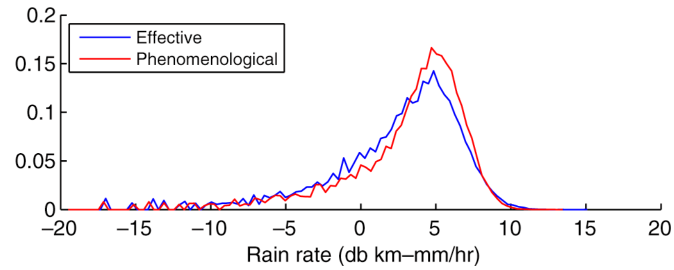

Fig. 7. Histograms of the rain estimates produced using both the effective and phenomenological rain models for a fixed speed of 10 m/s and rain rate of 3 km-mm/hr.

Before discussing the simulation results, it is important to understand the direction squared error. Because wind direction is a circular variable, the mean squared error between the true wind direction and the estimated wind direction is calculated as

$$MSE = n^{-1} \sum_{i=1}^{n} (\Delta_i)^2 \quad (24)$$

where i indexes the estimates and Δ_i is defined such that $|\Delta_i|$ is the lesser of $|\hat{d}_i - d_t|$ and $2\pi - |\hat{d}_i - d_t|$. $\hat{d}_i$ is the estimated wind direction and d_t is the true wind direction. Note that the maximum value of Δd_i is 180° and the minimum is −180°.

Generally, the root-mean-squared error for the wind vector estimates is very similar for either rain model. The largest differences between the two rain models are best seen in the distributions of estimated rain rates. Fig. 7 shows the distribution of estimated rain rates for a true wind speed of 10 m/s and a rain rate of 4.7 dB km-mm/hr. Interestingly, the phenomenological rain model has fewer low ($<$ 3 dB km-mm/hr) rain estimates and few higher ($>$ 7 dB km-mm/hr) rain estimates, which indicates a greater concentration of rain estimates; however, the bias in the phenomenological rain estimates is slightly larger. Before comparing real data, we apply the Monte Carlo results for the estimator bias to form the biased CRLB.

C. Theoretic Performance Limits

Fig. 8 shows the CRLB for a fixed wind speed and several rain rates as a function of true wind direction. It is immediately apparent that there are several wind directions which are problematic. For these wind directions, the standard deviation of the direction estimates are unrealistically high. This is one limitation of the QuikSCAT observation geometry. Winds that are parallel to the antenna azimuth angle are particularly noisy regardless of the swath location. Near these problematic wind directions, the error can be substantial enough to effectively mask all information about wind direction. This causes the Fisher information for wind direction to approach zero, thus causing the Fisher information matrix to approach singularity. For these wind directions, the near-singularity of the Fisher information matrix causes the bounds for wind speed and rain rate to be greatly overestimated.

Interestingly, although the CRLB does not give a physically meaningful result for these directions, in reality, there is a more realistic upper bound on the direction variance. Because wind

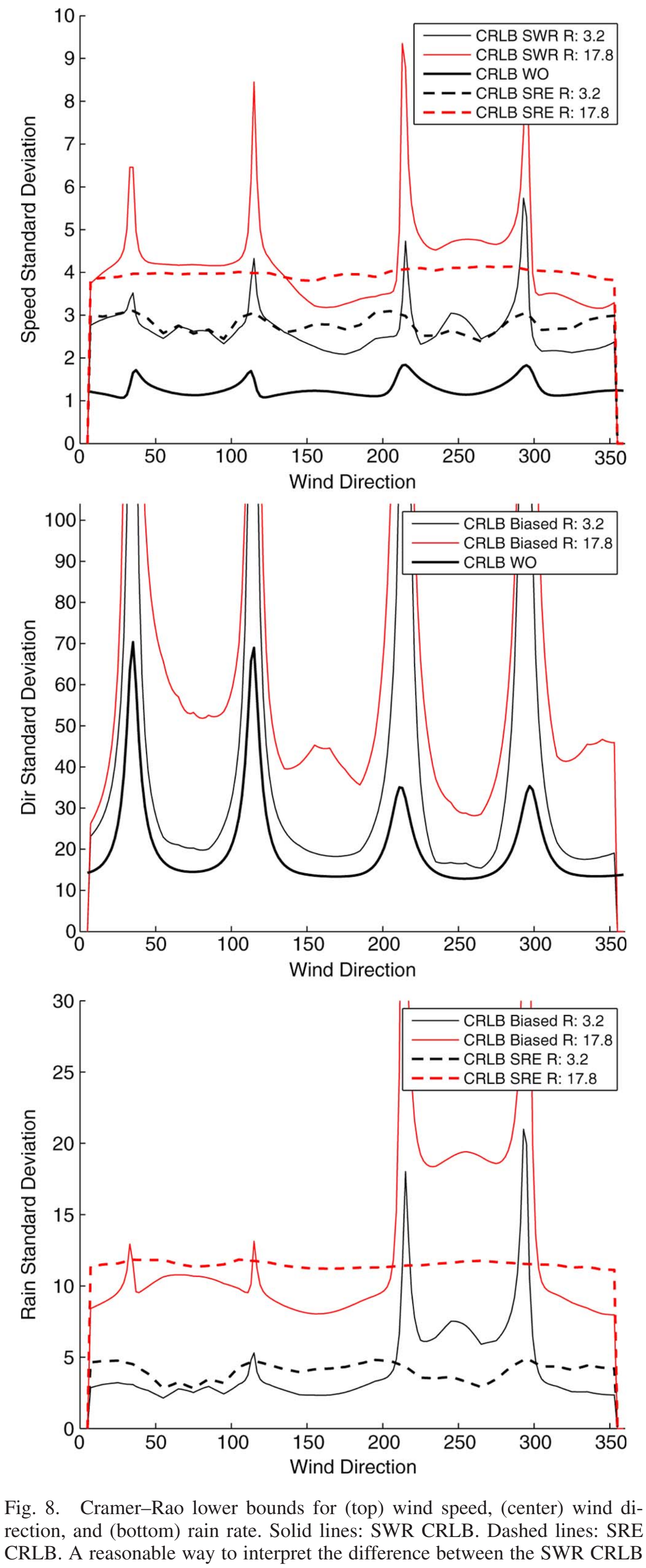

Fig. 8. Cramer–Rao lower bounds for (top) wind speed, (center) wind direction, and (bottom) rain rate. Solid lines: SWR CRLB. Dashed lines: SRE CRLB. A reasonable way to interpret the difference between the SWR CRLB and the SRE CRLB is to assume the overall CRLB is the smaller of the two bounds. In each case, these bounds correspond to a fixed wind speed of 10 m/s.

direction is only valid from 0 to 360°, there is a wrapping effect. This implies that a worst case direction estimate distribution is a uniform distribution from 0 to 360°. This effectively upper bounds the wind direction standard deviation at 103.9°, the

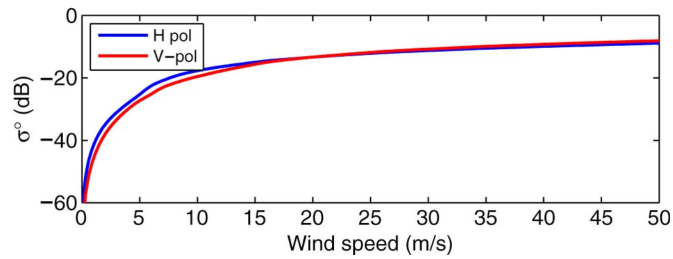

Fig. 9. Wind speed GMF for H and V polarizations.

standard deviation of a uniform distribution from 0 to 360. It may be possible to further reduce this upper bound by evaluating the effects of multiple ambiguities but we do not pursue this concept here.

In terms of the Fisher information, a standard deviation that exceeds 103.9° indicates that there is little direction information. When this is so, the Fisher information is nearly singular, making the speed and rain bounds inaccurate as well. We can obtain an alternative bound on wind speed and rain rate by formulating a separate wind speed and rain rate estimator. The wind speed and rain rate estimator (SRE) is particularly useful for cases where the QuikSCAT observation geometry is poorly suited to wind direction retrieval. In these cases, azimuthal dependence of the backscatter is ignored and wind speed and rain estimates can be made from the backscatter magnitude alone.

Because the SRE does not estimate wind direction, it remains valid as a lower bound, even when there is little or no direction information. Essentially, the CRLB for SRE can be used whenever the direction variability passes realistic limits (103.9°). Although, in reality, the retrieval process always includes a direction estimate, the retrieval process can be approximated by the SRE because the wind direction can be treated as if it is randomly chosen by the retrieval algorithm when there is no direction information.

The CRLB for the SRE is calculated in the same way as the SWR estimator. The principle difference is the model function. To approximate a wind speed and rain rate geophysical model, we can average the conventional wind vector GMF over wind direction. This gives a model for the wind speed which can be combined with the rain model using (19) as before. The wind speed GMF is shown in Fig. 9 for both H and V polarizations.

Although the CRLB indicates that it is not possible to reliably estimate the wind direction at ultra-high resolution for some particular true wind directions, for many of the most common wind and rain vectors, SWR estimation has similar performance to conventional UHR wind estimation. Further, accurate wind direction estimates can still be formed at the conventional QuikSCAT resolution [6], [20]. Additionally, it may still be possible to improve the direction estimates using a modified version of the directional interval retrieval algorithm proposed in [21], although this is not investigated here.

D. SWR Performance

It has been previously demonstrated that SWR retrieval at conventional (25 km) resolution can produce unbiased estimates of rain rate, although there is significant variance in the estimates [6], [12]. SWR estimation using UHR data has

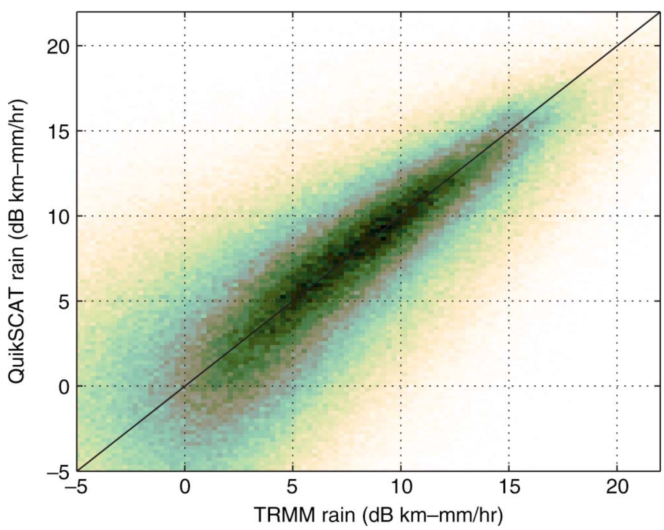

Fig. 10. Scatter density of QuikSCAT reference rain and TRMM PR-measured rain. The QuikSCAT sampling causes variability about the TRMM PR measurements but does not introduce a bias into the rain measurements.

several issues that require additional considerations. First is the issue of noise. At UHR, the noise level of the QuikSCAT observations is substantially greater than the conventional-resolution observations. The second issue is resolution. Note that although QuikSCAT UHR products are reported at 2.5 km, their effective resolution is somewhat coarser.

To make the dependence on temporal resolution and the QuikSCAT sampling pattern clear, we attempt to separate the effects of each as we compare the estimation results. To isolate the effects of observation noise, we can define a reference rain field which accounts for the resolution of the QuikSCAT UHR observations. This reference rain field is the rain field that QuikSCAT would observe if it made noiseless measurements with its sampling geometry. The comparison of the reference rain field and the QuikSCAT rain estimates gives an indication of the ability of QuikSCAT sampling to detect and estimate the rain from high-noise observations.

Just as in the backscatter modeling, there are two types of resolution in wind and rain estimation, temporal and spatial, the effects of which we must include in defining an appropriate reference rain field. To account for spatial resolution and sampling, we use the rain field defined by (9) for each observation flavor. To account for QuikSCAT temporal sampling effects, we use the constant shift approximation introduced in Section III-B calculated using the cross-correlation. The shifts are then applied to the rain field for each flavor. There are thus four separate rain fields which are sampled and shifted copies of the TRMM PR-observed rain field. These four rain fields thus represent the rain field observed by each QuikSCAT observation flavor.

To assimilate these four different rain fields into a single rain field requires one final assumption. By assuming that each QuikSCAT flavor contributes equally to the overall rain estimate, an overall reference rain field can be created by averaging the four separate rain fields. While there may be an optimal weighting of the four rain fields that could better reflect the sensitivity of a particular polarization to rain, this approximation is simple and yields a good reference rain field without additional complications. We define the reference rain field to be

$$R_{QSCAT} = (R_{VF} + R_{HF} + R_{HA} + R_{VA})/4 \tag{25}$$

where R_{VF}, R_{HF}, R_{HA}, and R_{VA} are time-shifted versions of the rain fields calculated using (9), and R_{QSCAT} is the reference rain field for QuikSCAT that accounts for both temporal and spatial sampling effects. Fig. 10 shows the scatter density plot of QuikSCAT reference winds and TRMM PR-measured winds. As might be hoped for, the QuikSCAT sampling process does not cause any overall bias for most rain measurements.

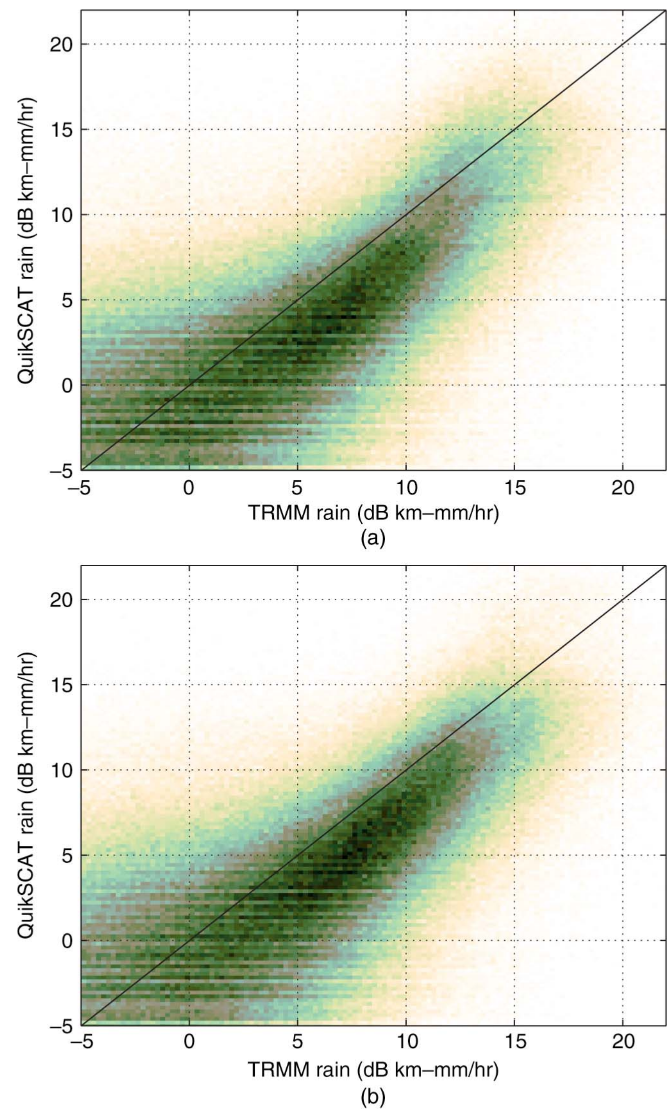

Fig. 11. Scatter density plots of QuikSCAT reference rain rates and QuikSCAT retrieved rain rates for (a) the effective rain model and (b) phenomenological rain model. The equality line is shown for comparison. The rain estimates are biased low for both models. Overall, the rain estimation performance using either model is very similar.

With the combined effects of spatial and temporal sampling accounted for, the remainder of the variability in the rain estimates can be attributed primarily to observation noise. Fig. 11

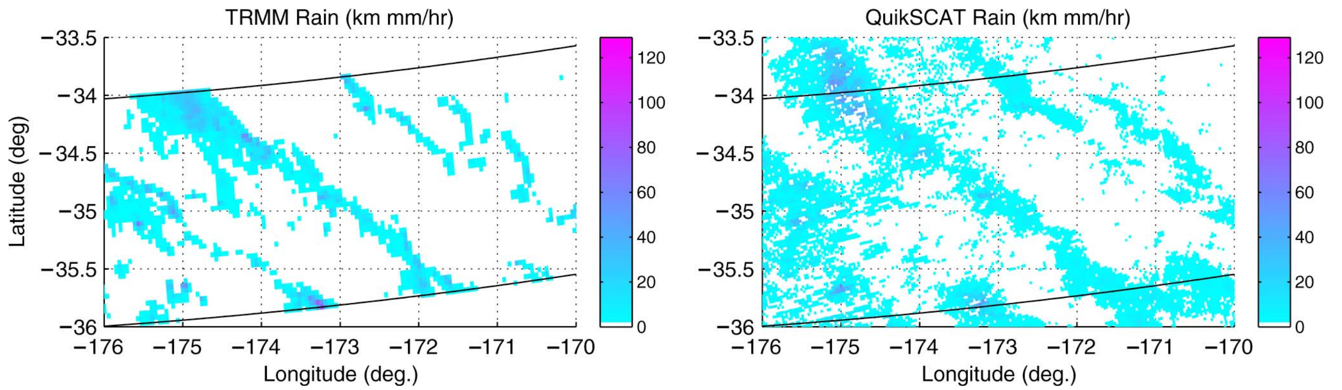

Fig. 12. (Left) TRMM PR-measured rain rate and (right) QuikSCAT-estimated rain rate for one overlapping region. TRMM swath edges are indicated by the black lines. Although QuikSCAT fails to detect the lowest rain rates and is noisy, the spatial correlation of the two data sets is quite apparent. The rain rate color scale for this image ranges from 0 to 132 km-mm/hr.

shows the scatter density plots for QuikSCAT rain estimates and TRMM PR rain rates at UHR for both rain models. The rain estimates are biased slightly low for all rain rates using both models, but this bias can be minimized by bias-correcting the rain estimates. The most prominent feature of Fig. 11, unfortunately, is the high standard deviation of the QuikSCAT rain estimates, which can exceed 5 dB km-mm/hr. Such a high variance level may be intolerable in many applications; however, although we do not consider it here, resolution reduction can decrease estimate variability by reducing observation noise [22].

Some effects that are not apparent in the scatter density are noise effects such as spurious rain estimates and missing wind estimates. Both of these are an inherent part of SWR estimation and occur as a consequence of the smoothness of the likelihood function. At times, the maximum of the likelihood function is so flat that the maximum can be overlooked by the search algorithm. There are also times when there is no local maximum in the wind and rain space so that no SWR estimates can be made. Typically, this occurs when the wind or the rain signal is dominated and obscured by the other.

Although the rain estimate variability is high, one important observation about QuikSCAT rain estimates not apparent in Fig. 11 is the ability of QuikSCAT to identify the general structure of rain events at high resolution. To demonstrate this ability, Fig. 12 shows the TRMM PR-measured rain rates and QuikSCAT SWR rain estimates for a case study. Fig. 12 indicates that although there are spurious and missing rain estimates, the QuikSCAT rain estimates correctly identify the rain bands observed by TRMM PR. This ability is useful as a rain flag on the wind data, particularly when collocated TRMM PR data is not available, and can be used to select areas where a rain-only estimator should be used, overcoming the spurious rain characteristics that occur when wind backscatter signal is entirely obscured by rain, see [23].

VI. Buoy Validation

Prior results have validated the accuracy of QuikSCAT-estimated rain rates against TRMM PR observations. However, a principle advantage of SWR is the improvements it produces for wind estimation during raining conditions [6]. Lacking a source of high-resolution wind field measurements, we evaluate the wind measurement performance in the presence of rain against collocated buoy measurements. Buoy validation of non-rain contaminated UHR winds estimated using a WO retrieval algorithm is considered in [24].

As few ocean buoys provide reliable rain measurements, we identify raining conditions at the time of the QuikSCAT overpass of each buoy based on the IMUDH rain indicator contained in QuikSCAT L2B files. The IMUDH indicator is a modified version of the MUDH rain flag [2] designed to indicate the likelihood of rain-impact on a given 25 km wind estimate [25]. The value of the IMUDH indicator increases with increasing rain impact.

Data from 30 buoys located at least 50 km from land during 2003 were considered, resulting in nearly 1000 buoy and QuikSCAT colocations with at least some level of rain contamination as determined by either a non-zero IMUDH flag or a non-zero UHR SWR rain estimate. For these raining wind observations, we contrast QuikSCAT UHR winds with buoy winds in Figs. 13 and 14 for two cases: SWR and WO. The statistics are summarized in Table II where they are compared with conventional 25-km resolution QuikSCAT L2B winds. In all cases, the scatterometer wind ambiguity closest to the buoy-observed wind direction is selected.

Comparison of the results reveals that UHR SWR has reduced wind speed bias and variability compared to either UHR WO or L2B, and thus the SWR wind speed is more accurate. While the SWR has slightly lower wind direction bias, the SWR RMS direction error is larger than either UHR WO or L2B. This results from the fact that both UHR WO and L2B have more wind direction ambiguities to select from than does UHR SWR, which often has only a single ambiguity. The single ambiguity causes the large off-diagonal scatter in SWR wind direction in Fig. 14. Since UHR SWR provides improved wind speed estimates but not improved wind directions in the single ambiguity case, one approach is to use the SWR-derived wind speed and WO-derived wind direction.

We note that for rainy conditions the UHR WO wind speed and direction errors are smaller than L2B. This results from the improved resolution of the UHR WO and correspondingly lower adverse beam filling effects from rain as well as from the

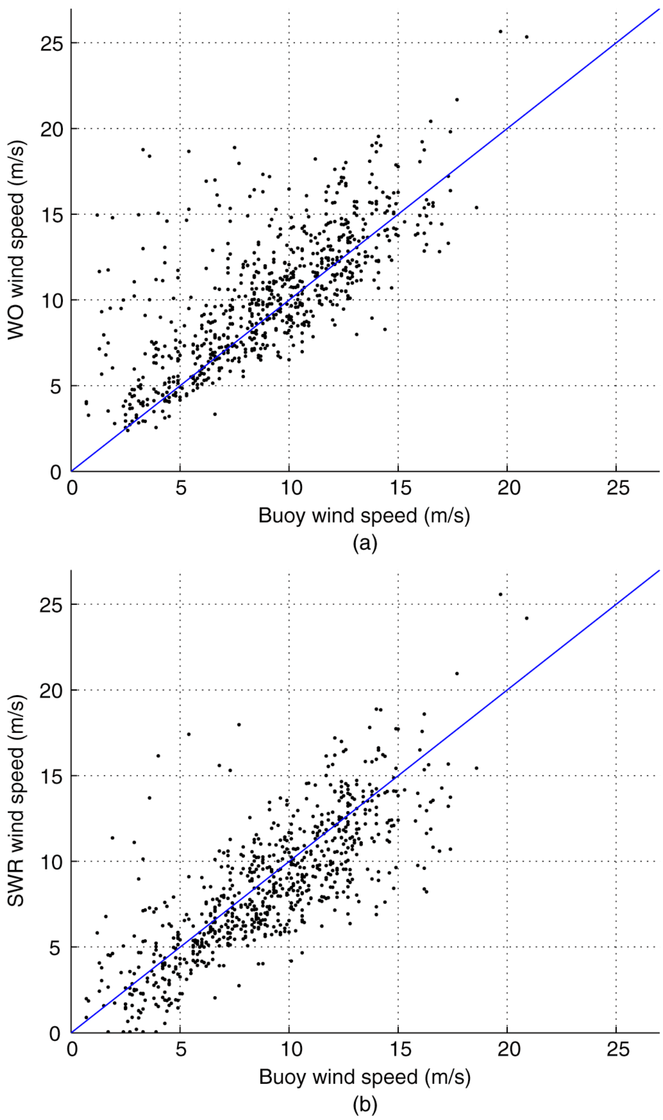

Fig. 13. (a) QuikSCAT WO and (b) SWR wind speed estimates as a function of measured buoy wind speed for rain perturbed observations. The WO wind estimates are biased while the SWR wind estimates have reduced overall bias and fewer estimates with severe errors.

fact that L2B directions in the presense of rain tend to be biased toward 90 and 270 degrees relative to the spacecraft nadir track [6].

A quantitative comparison of the root-mean-squared error between the buoy measurements and the QuikSCAT wind estimates versus the IMUDH value is shown in Fig. 15. The plot includes 25-km (L2B) QuikSCAT winds. Note that as the IMUDH value increases and rain contamination becomes more likely, the WO and L2B RMS error and bias increase. However, the SWR bias and RMS error shows little variation with IMUDH value. On average, in rainy conditions, SWR produces more accurate wind estimates than does WO retrieval, see Table II. However, since WO winds are more accurate than SWR winds when there is no rain contamination, optimum performance can be achieved by reporting SWR winds in rainy conditions when the SWR-estimated rain rate is non-zero and WO wind estimates when there is no rain. Optimum estimator-selection-based wind and rain conditions are explored in [23].

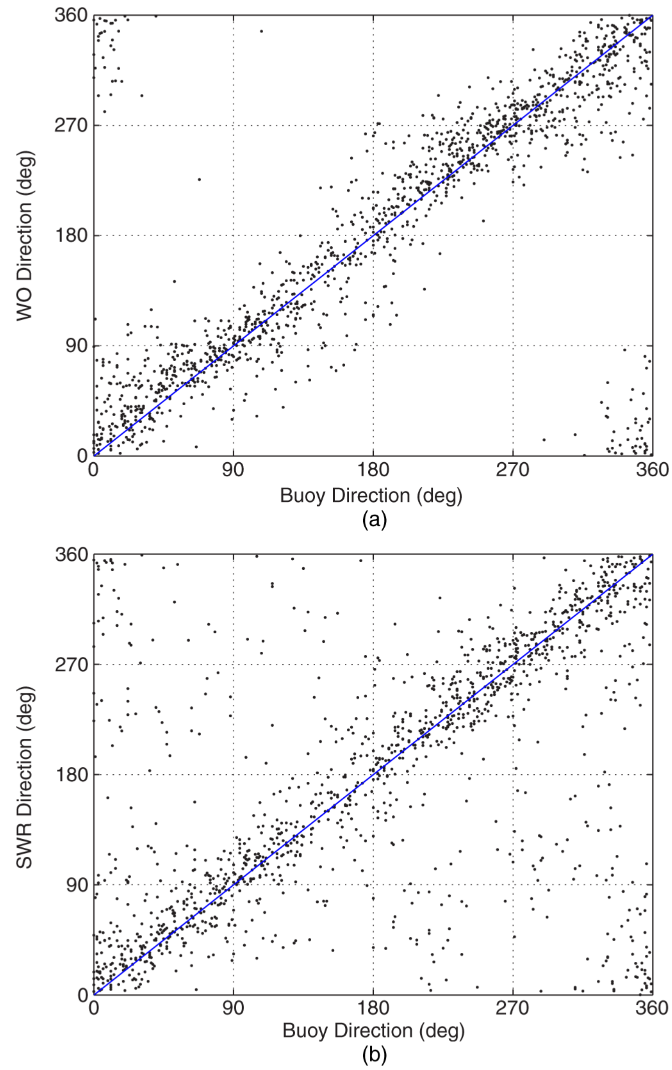

Fig. 14. (a) QuikSCAT WO and (b) SWR wind direction estimates as a function of measured buoy direction for rain perturbed observations. see text.

TABLE II
SUMMARY OF QUIKSCAT MINUS BUOY WIND SPEED DIFFERENCES

QuikSCAT	Speed (m/s)		Direction (deg)	
Product	Bias	RMS	Bias	RMS
UHR SWR	0.07	3.05	1.6	57.0
UHR WO :	3.05	5.01	-0.8	36.6
25 km L2B	5.14	6.51	-3.6	34.8

VII. CONCLUSION

We have found that the effective and phenomenological rain models are both reasonable approaches to modeling the effects of rain on QuikSCAT UHR backscatter data. As neither model is manifestly superior based on the available data sets, the phenomenological rain model may be a better choice for rain estimation as it more realistically models extreme rain events where atmospheric backscatter is dominant.

Our results demonstrate that QuikSCAT is capable of measuring the wind and rain simultaneously at UHR. UHR wind and rain estimates offer insights into wind and rain events at resolutions that are not achievable using any other single sensor. These insights can aid in understanding important phenomena

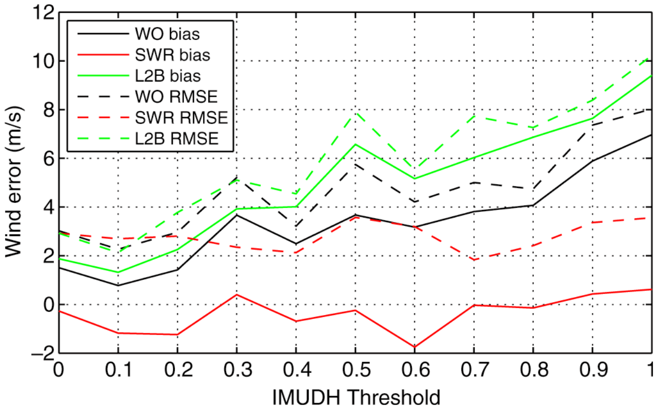

Fig. 15. Wind speed bias and RMS error for 25-km L2B winds, and 2.5-km WO and SWR wind estimates as a function of the IMUDH threshold. The IMUDH rain flag specifies the probability that a wind vector is perturbed by more than 2 m/s by rain effects. The SWR wind estimates have lower bias and RMS error than both the WO and L2B winds for all IMUDH values. Rain-free observations are not included in this plot.

such as hurricanes and other large-scale convective storms. This ability is particularly useful in regions outside the tropics which are not observed by TRMM PR or similar instruments. Thus despite high levels of noise, the QuikSCAT UHR wind and rain product is potentially a valuable tool in understanding mesoscale phenomena.

REFERENCES

[1] C. A. Mears, D. K. Smith, and F. J. Wentz, "Detecting rain with QuikSCAT," in *Proc. IGARSS*, 2000, pp. 1235–1237.

[2] J. N. Huddleston and B. W. Stiles, "A multidimensional histogram rain-flagging technique for SeaWinds on QuikSCAT," in *Proc. IGARSS*, Jul. 2000, vol. 3, pp. 1232–1234.

[3] M. Portabella and A. Stoffelen, "Rain detection and quality control of SeaWinds," *J. Atmos. Ocean. Technol.*, vol. 18, no. 7, pp. 1171–1183, Jul. 2001.

[4] B. W. Stiles and S. H. Yueh, "Impact of rain on spaceborne Ku-band wind scatterometer data," *IEEE Trans. Geosci. Remote Sens.*, vol. 40, no. 9, pp. 1973–1983, Sep. 2002.

[5] D. E. Weissman, M. A. Bourassa, J. J. O'Brien, and J. S. Tongue, "Calibrating the QuikSCAT/SeaWinds radar for measuring rainrate over the oceans," *IEEE Trans. Geosci. Remote Sens.*, vol. 42, no. 7, pp. 2814–2820, Jul. 2004.

[6] D. Draper and D. Long, "Simultaneous wind and rain retrieval using SeaWinds data," *IEEE Trans. Geosci. Remote Sens.*, vol. 42, no. 7, pp. 1411–1423, Jul. 2004.

[7] D. Long, J. Luke, and W. Plant, "Ultra high resolution wind retrieval from SeaWinds," in *Proc. IGARSS*, 2003, pp. 1264–1266.

[8] M. H. Freilich and R. S. Dunbar, "Derivation of satellite wind model functions using operational surface wind analyses: An altimeter example," *J. Geophys. Res.*, vol. 98, no. C8, pp. 14 633–14 649, Aug. 1993.

[9] B. A. Williams and D. G. Long, "A reconstruction approach to scatterometer wind vector field retrieval," *IEEE Trans. Geosci. Remote Sens.*, vol. 49, no. 6, pp. 1850–1864, Jun. 2011.

[10] D. G. Long and M. W. Spencer, "Radar backscatter measurement accuracy for a spaceborne pencil-beam wind scatterometer with transmit modulation," *IEEE Trans. Geosci. Remote Sens.*, vol. 35, no. 1, pp. 102–114, Jan. 1997.

[11] F. M. Naderi, M. H. Freilich, and D. G. Long, "Spaceborne radar measurement of wind velocity over the ocean—An overview of the NSCAT scaterometer system," *Proc. IEEE*, vol. 76, no. 6, pp. 850–866, Jun. 1991.

[12] D. Draper and D. Long, "Assessing the quality of SeaWinds rain measurements," *IEEE Trans. Geosci. Remote Sens.*, vol. 42, no. 7, pp. 1424–1432, Jul. 2004.

[13] R. F. Contreras, W. J. Plant, W. C. Keller, K. Hayes, and J. Nystuen, "Effects of rain on Ku-band backscatter from the ocean," *J. Geophys. Res.*, vol. 108, no. C5, pp. 34-1–34-13, May 2003.

[14] B. L. Mehaute and T. Khangaonkar, "Dynamic interaction of intense rain with water waves," *J. Phys. Oceanogr.*, vol. 20, no. 12, pp. 1805–1812, Dec. 1990.

[15] S. N. Nielsen and D. G. Long, "A wind and rain backscatter model derived from AMSR and SeaWinds data," *IEEE Trans. Geosci. Remote Sens.*, vol. 47, no. 6, pp. 1595–1606, Jun. 2009.

[16] I. Ashcraft and D. Long, "The spatial response function of SeaWinds backscatter measurements," in *Proc. SPIE—Earth Observing Systems VIII*, W. L. Barnes, Ed., Aug. 3–6, 2003 , vol. 5151, pp. 609–618.

[17] R. K. Crane, *Electromagnetic Wave Propagation Through Rain*. New York: Wiley, 1996.

[18] I. Strangeways, *Precipitation: Theory, Measurement and Distribution*. Cambridge, U.K.: Cambridge Univ. Press, 2007.

[19] D. Draper and D. Long, "Evaluating the effect of rain on SeaWinds scatterometer measurements," *J. Geophys. Res.*, vol. 109, no. C12, pp. C02 005.1–C02 005.12, Feb. 2004.

[20] T. E. Oliphant and D. G. Long, "Accuracy of scatterometer-derived winds using the Cramér-Rao bound," *IEEE Trans. Geosci. Remote Sens.*, vol. 37, no. 6, pp. 2642–2652, Nov. 1999.

[21] B. W. Stiles, B. D. Pollard, and R. S. Dunbar, "Direction interval retrieval with threshold nudging: A method for improving the accuracy of QuikSCAT winds," *IEEE Trans. Geosci. Remote Sens.*, vol. 40, no. 1, pp. 79–89, Jan. 2002.

[22] M. P. Owen and D. G. Long, "Progress toward validation of QuikSCAT ultra-high-resolution rain rates using TRMM PR," in *Proc. IGARSS*, Jul. 2008, vol. 4, pp. 299–302.

[23] M. P. Owen and D. G. Long, "Towards Bayesian estimator selection for QuikSCAT wind and rain estimation," in *Proc. IGARSS*, Jul. 2010, pp. 1331–1334.

[24] A. M. Plagge, D. C. Vandemark, and D. G. Long, "Coastal validation of ultra-high resolution wind vector retrieval from QuikSCAT in the Gulf of Maine," *IEEE Geosci. Remote Sens. Lett.*, vol. 6, no. 3, pp. 413–417, Jul. 2009.

[25] *QuikSCAT Science Data Product User's Manual*, Phys. Oceanogr. DAAC, JPL, Pasadena, CA, 2006, D-18053.

Michael P. Owen received the B.S. degree in electrical engineering from Brigham Young University (BYU), Provo, UT, in 2007, where he received the Ph.D. degree in electrical engineering, in September 2010 after completing his dissertation titled "Scatterometer Contamination Mitigation".

He worked in the Microwave Earth Remote Sensing Laboratory, from 2006 to 2010, working toward rain backscatter modeling, simultaneous wind and rain estimation, and Bayesian decision theory applications to ultra-high-resolution scatterometry. He is currently at the MIT Lincoln Laboratory.

David G. Long (S'80–SM'98–F'08) obtained the Ph.D. degree in electrical engineering from the University of Southern California, Los Angeles, in 1989.

From 1983 to 1990, he worked for NASA's Jet Propulsion Laboratory (JPL), Pasadena, CA, where he developed advanced radar remote sensing systems. While at JPL, he was the Project Engineer on the NASA Scatterometer (NSCAT) project which flew from 1996 to 1997. He also managed the SCANSCAT project, the precursor to SeaWinds which was launched in 1999 on QuikSCAT and 2002 on ADEOS-II. He is currently a Professor in the Electrical and Computer Engineering Department at Brigham Young University, Provo, UT, where he teaches upper division and graduate courses in communications, microwave remote sensing, radar, and signal processing and is the Director of the BYU Center for Remote Sensing. He is the Principal Investigator on several NASA-sponsored research projects in remote sensing. He has 390 publications in various areas including signal processing, radar scatterometry, and synthetic aperature radar. His research interests include microwave remote sensing, radar theory, space-based sensing, estimation theory, signal processing, and mesoscale atmospheric dynamics. He has received the NASA Certificate of Recognition several times. He is an Associate Editor for IEEE GEOSCIENCE AND REMOTE SENSING LETTERS.